How to cite: *Angew. Chem. Int. Ed.* **2022,** *61,* e202211562
International Edition: doi.org/10.1002/anie.202211562
German Edition: doi.org/10.1002/ange.202211562

Reduction

Discovery of a Thioxanthone–TfOH Complex as a Photoredox Catalyst for Hydrogenation of Alkenes Using *p*-Xylene as both Electron and Hydrogen Sources

Wen-Jie Kang, Bo Li, Meng Duan, Guangxing Pan, Weiqiang Sun, Aishun Ding, Yanbin Zhang, K. N. Houk,* and Hao Guo**

Abstract: Hydrogenation of alkenes is one of the most fundamental transformations in organic synthesis, and widely used in the petrochemical, pharmaceutical, and food industries. Although numerous hydrogenation methods have been developed, novel types of catalysis with new mechanisms and new hydrogen sources are still desirable. Thioxanthone (TX) is widely used in energy-transfer photoreactions, but rarely in photoredox processes. Herein we show that a catalytic amount of TfOH as a co-catalyst can tune the properties of TX to make it a photoredox catalyst with highly enhanced oxidative capability in the hydrogenation of carbonylated alkenes with the cheap petroleum industrial product *p*-xylene serving as the hydrogen source. Deuterium can also be introduced by this method by using D_2O as the D source. To the best of our knowledge, this is the first example of using *p*-xylene as a hydrogen source.

Introduction

The hydrogenation of alkenes is one of the most fundamental transformations in organic synthesis and can be traced back as early as the 1912 Nobel Prize to Sabatier (shared with Grignard).[1] It is widely used in the petrochemical industry, the pharmaceutical industry and the food industry.[2] Hydrogenation of alkenes normally requires a combination of a catalyst and a corresponding hydrogen source (Figure 1a). Conventional hydrogenation transition-metal catalysts include Pd/C,[3] the Wilkinson catalyst,[4] the Crabtree catalyst,[5] the Lindlar catalyst,[6] and Raney nickel.[7] Other metal-centered complexes, such as Rh,[8] Ni,[9] Ir,[10] Cu,[11] Fe,[12] Mn,[13] Co,[14] Ba,[15] and V complexes,[16] have also been developed as hydrogenation catalysts. Notably, heterogeneous hydrogenation catalysts are critical and widely used in industry.[17] With the development of well-defined ligands, both homogeneous and heterogeneous asymmetric hydrogenation reactions are also developing rapidly.[18] A breakthrough in organocatalytic hydrogenation was the discovery by the Stephan group of frustrated Lewis pairs (FLPs),[19] which form stable B–H and

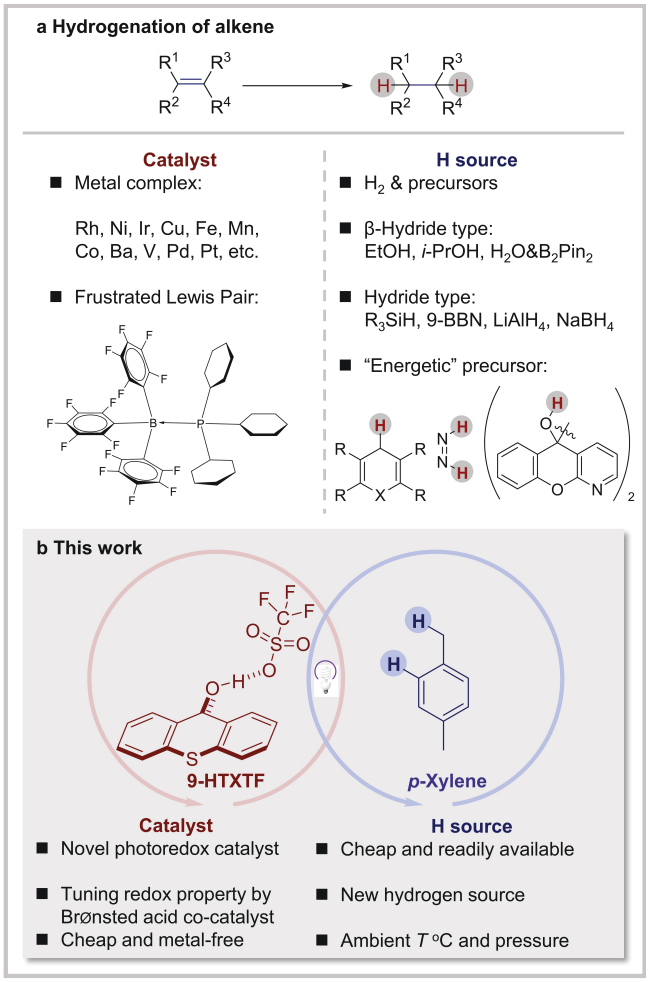

Figure 1. Hydrogenation reactions.

[*] W.-J. Kang, G. Pan, W. Sun, Dr. A. Ding, Dr. Y. Zhang, Prof. Dr. H. Guo
Department of Chemistry,
Fudan University
2005 Songhu Road, Shanghai 200438 (PR China)
E-mail: zhangyb15@fudan.edu.cn
Hao_Guo@fudan.edu.cn
B. Li, Dr. M. Duan, Prof. Dr. K. N. Houk
Department of Chemistry and Biochemistry
University of California, Los Angeles
Los Angeles, California 90095 (USA)
E-mail: houk@chem.ucla.edu

P–H intermediates with H_2, for the hydrogenation of alkenes, alkynes, imines, and other compounds.[20] Although the catalyst plays an essential role in hydrogenation reactions, the hydrogen source is also an indispensable component (Figure 1a). The most common hydrogen source is hydrogen gas (H_2), which is an ideal hydrogen source with 100 % atom efficiency. However, there are still potential safety concerns in handling flammable and explosive H_2, and various active hydrogen sources have been developed for hydrogenation reactions. Typically, H_2 precursors, such as HCO_2H[21] and HCO_2NH_4,[3,22] have been developed as alternatives. Metal-hydride formation by β-hydride elimination from readily accessible hydrogen sources, such as EtOH,[23] *i*-PrOH,[24] H_2O–B_2Pin_2,[25] was also a significant advance. Notably, D_2O–B_2Pin_2 can also be used to introduce deuterium during the hydrogenation process, providing a convenient synthesis of deuterated organic compounds. 9-BBN, $LiAlH_4$, and $NaBH_4$[26] are representative examples of hydride-type hydrogen sources. Their nucleophilicity causes them to behave as useful hydrogen sources in hydrogenation reactions, especially for the reduction of polarized alkenes. Finally, a type of "energetic" precursor can release hydrogen with a high thermodynamic driving force by concomitant aromatization[27] or entropy increase.[28] These reagents are powerful hydrogen sources, especially for "non-metal-hydride-mediated" hydrogenation reactions. Although numerous methods employing different types of catalysts and relatively active hydrogen sources have been developed, catalytic methods with novel mechanisms and new hydrogen sources are still desirable.

Photochemistry[29] provides a relatively new approach to substrate activation. The direct photoexcitation of a metal hydride intermediate may facilitate hydride transfer to unsaturated bonds, enabling the hydrogenation of alkenes and aromatic compounds.[30] In the case of photoredox catalysis, the excited photocatalyst has enhanced redox potential as compared to its ground state. Photoredox catalysis has been applied to the hydrogenation of aromatic compounds and electron-deficient alkenes by using *N*,*N*-diisopropylethylamine, or Hantzsch esters as the hydrogen source, respectively.[31] With the assistance of an "Ene"-reductase, NADPH could also be used in photoredox hydrogenation.[32] However, photoredox catalytic hydrogenation reactions are limited to ruthenium- or iridium-based complexes and organic amines as both electron and hydride donor. Novel photochemical hydrogenation catalysts and hydrogen sources are highly desirable. Herein, we report our recent discovery of a photochemical hydrogenation reaction using 9-hydroxy-9*H*-thioxanthen-9-ylium trifluoromethanesulfonate (**9-HTXTF**) as a catalyst and *p*-xylene as the hydrogen source (Figure 1b).

Results and Discussion

In initial studies, we observed that the colorless TX solution turned bright yellow upon the addition of TfOH, indicating the formation of a new species, **9-HTXTF**, whose structure was first determined by single-crystal X-ray diffraction (Figure 2a).[33] Next, UV/Vis spectroscopy studies found that **9-HTXTF** had a new absorption band in the 400–450 nm region (Figure 2b). ^{1}H NMR spectroscopic analysis showed that the peaks of **9-HTXTF** were shifted dramatically downfield (Figure 2c). In both fluorescence and phosphorescence spectra, red-shifted peaks were observed for **9-HTXTF** as compared to TX (Figure 2d). Furthermore, the photophysical properties of **9-HTXTF** showed that its singlet lifetime was significantly extended ($\tau_s = 10.8$ ns), while its triplet lifetime was slightly shortened ($\tau_t = 1.0$ ms) as compared to TX (Figure 2e,f). Cyclic voltammetry measurement supported the hypothesis that **9-HTXTF*** had a dramatically enhanced oxidative capability ($E_{1/2}$(**9-HTXTF***/**9-HTXTF**$^{\bullet-}$) = +2.53 V vs. SCE) as compared to TX ($E_{1/2}$(TX*/TX$^{\bullet-}$) = +1.54 V vs. SCE; Figure 2g). Notably, its oxidative capability was stronger than that of photoredox catalyst Mes–Acr–BF_4 ($E_{1/2}$(Mes–Acr–BF_4*/Mes–Acr–$BF_4^{\bullet-}$) = +2.15 V vs. SCE).[34] Ultimately, computational studies using (time-dependent) density functional theory indicated that **9-HTXTF** had a lower photocatalyst excitation energy than TX, so it could be excited more easily by visible light (Figure 2h). These results suggested that **9-HTXTF** might act as a new photoredox catalyst with a sufficiently long singlet lifetime, adequately strong oxidation potential, and relatively facile photoexcitation ability.

An initial attempt was carried out with *N*,3-dimethyl-*N*-phenylbut-2-enamide (**19S**) as the model substrate. The hydrogen source was first examined in the presence of 10 mol% of thioxanthone (TX) and 10 mol% of TfOH at room temperature under photoirradiation ($\lambda = 404$ nm; Table S1, entries 1 and 2). The results revealed that both toluene and *p*-xylene could be used as the hydrogen source. Considering that reaction in *p*-xylene gave a better yield of the hydrogenation product *N*,3-dimethyl-*N*-phenylbutanamide (**19**), *p*-xylene was chosen as the hydrogen source. Subsequent solvent screening demonstrated that dichloromethane (DCM)/*p*-xylene (1:1) was the best solvent (Table S1, entries 3–7). When DCM/toluene (1:1) was used as the solvent, the reaction could also proceed slowly (Table S1, entry 8). Notably, when utilizing pure DCM or MeCN as the solvent, the target product **19** was not detected, which indicated that DCM or MeCN in the mixed solvent could not act as the hydrogen source (Table S1, entries 9 and 10). A series of acids were next tested. With decreasing acidity, a corresponding decrease in efficiency was observed (Table S1, entries 11–15), which indicated that the acidity played a crucial role in this hydrogenation. This phenomenon might be attributed to the stronger activation of TX by a stronger acid. DFT calculations suggested that, whereas the strong acid TfOH protonated TX, MsOH as an analogous yet marginally weaker acid could only form a hydrogen bond with TX. Therefore, TfOH ($pK_a = -14$) was chosen as the co-catalyst for further studies. Optimization of the loading of catalyst and co-catalyst demonstrated that 2.5 mol% of TX and 5 mol% of TfOH were optimal for this reaction (Table S1, entries 16–20). Notably, the reaction could be accelerated with a higher catalyst loading (Table S1, entry 21). When $(Ir[dF(CF_3)ppy]_2(dtbpy))PF_6$,[35] $Ru(bpy)_3Cl_2 \cdot 6H_2O$,[36] and [Ir(dF($CF_3$)ppy)$_2$(5,5′-d-

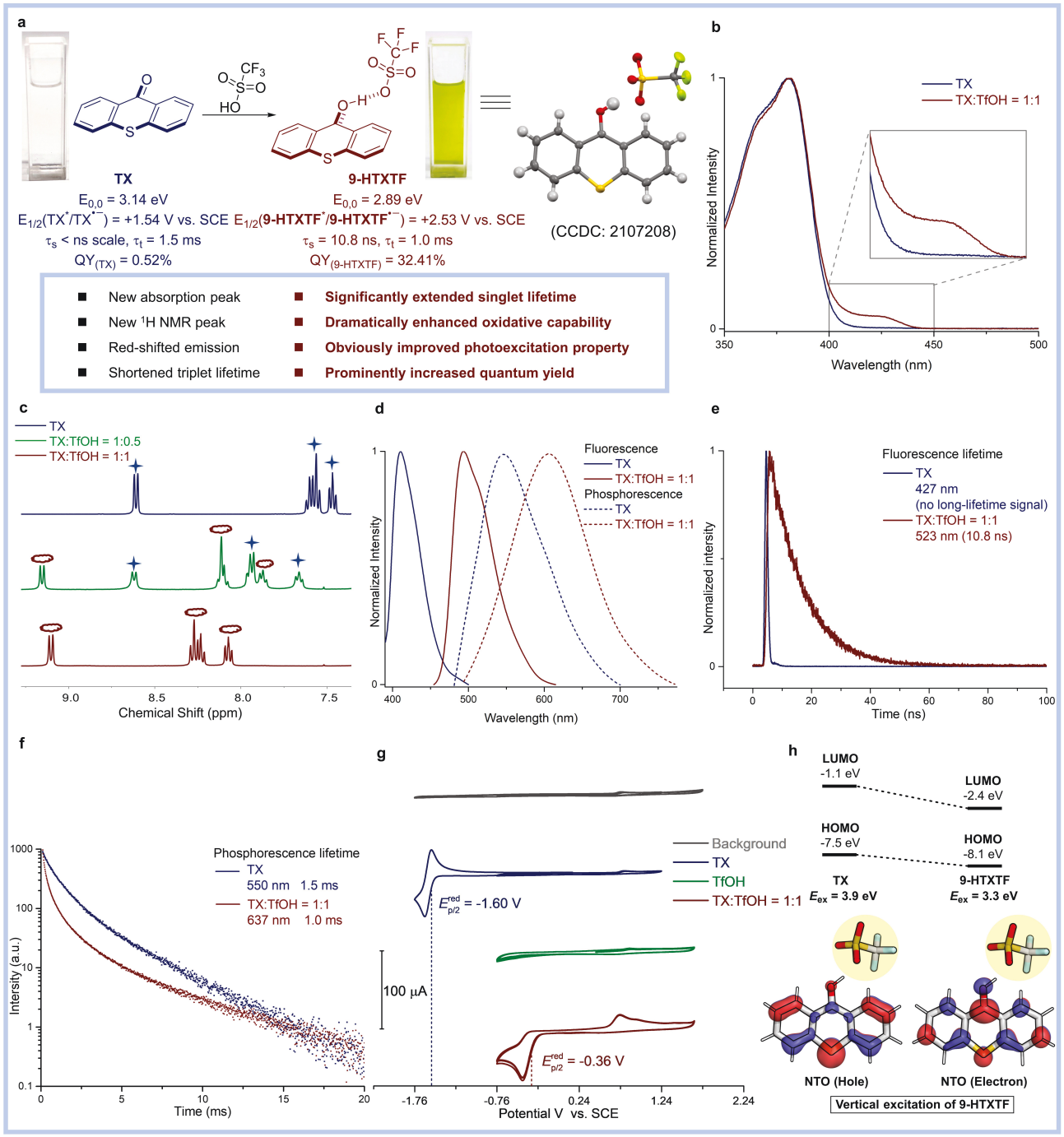

Figure 2. Properties of the **9-HTXTF** catalyst. a) The formation of **9-HTXTF**. b) Absorbance profiles for TX and TX:TfOH = 1:1 in DCM (0.05 mM). c) ^{1}H NMR spectra of TX, TX:TfOH = 1:0.5, and TX:TfOH = 1:1 (400 MHz, $CDCl_3$). d) Fluorescence emission spectra (λ_{ex}(TX) = 388 nm, λ_{ex}(TX:TfOH = 1:1) = 440 nm) collected in DCM (0.1 mM) and phosphorescence emission spectra (λ_{ex} = 380 nm) measured in solid form (after concentration of a solution of TX:TfOH = 1:1 in DCM under reduced pressure) . e) Fluorescence lifetime profiles for TX and TX:TfOH = 1:1 in DCM (0.1 mM). f) Phosphorescence lifetime measured as a solid (after concentration of a solution of TX:TfOH = 1:1 in DCM under reduced pressure). g) Cyclic voltammetry (for details, see the Supporting Information). h) Excited-state energies calculated using the TD-DFT method for TX and **9-HTXTF**. QY = quantum yield (for details, see the Supporting Information).

$(CF_3)bpy)]PF_6$[37] used in proton-coupled electron transfer (PCET) utilized as photocatalysts, no corresponding hydrogenation product was obtained in the photochemical reaction of **19S** (Table S1, entries 22–24). Moreover, other photoredox catalysts, such as 4-CzIPN, Eosin Y, and 9-mesityl-10-methylacridinium perchlorate, also did not show any catalytic activity (Table S1, entries 25–27). These results highlighted the uniqueness of the **9-HTXTF** catalyst. Normally, heterogeneous Ni and Pd are the best catalysts for hydrogenation of unsaturated carbonyl compounds in the

presence of H_2.[38] However, the discovery of catalyst **9-HTXTF** avoids the use of flammable and explosive H_2, since the cheap petroleum industry product *p*-xylene is utilized as the hydrogen source. Control experiments indicated that light, TX, and TfOH were required for any reaction (Table S1, entries 28–30). No reaction occurred at 60 °C without light (Table S1, entry 31). Hence, the optimal conditions (Table S1, entry 19) were chosen as the standard conditions for further studies.

Having optimized the reaction conditions, we carefully examined the scope of this photochemical hydrogenation reaction (Figure 3). A broad range of *N*-methylquinolone substrates containing substituents with different electronic effects gave the desired products **1**–**7** in excellent yield. 5-Methoxycarbonyl-substituted quinolone **8** was obtained in moderate yield, probably owing to hydrolysis of the ester group. Reactants with various substituted *N*-benzyl groups were also tested (products **9**–**14**). The benzylic proton in those substrates did not serve as hydrogen source and were thus nicely tolerated. Unprotected or *N*-phenyl quinolones were also tolerated (products **15**–**17**). Selective hydrogenation of the electron-deficient alkene moiety was observed when pirfenidone was used as the substrate (product **18**). No over-hydrogenated product was formed even when the hydrogen source was used in excess. Acyclic α,β-unsaturated amides can also be hydrogenated under these reaction conditions (products **19**–**22**). Menthol, adamantanol and borneol motifs were all stable under these conditions and did not affect the reactivity (products **23**–**25**). Carboxylic acids and ketones with electronically differentiated substitutes could also deliver products **26**–**35** in moderate to excellent yields. Coumarin derivatives with diverse functional groups were also competent (products **36**–**39**). Other esters, including a tetrasubstituted ester, were also transformed efficiently in this hydrogenation reaction (products **40**–**43**).

Then, we tried to demonstrate the application of this hydrogenation protocol to complex bioactive molecules (Figure 4). Dihydrofinasteride (**44**), which plays an important role in understanding the inhibition mechanism of finasteride, can be directly synthesized by the post-hydrogenation of Finasteride using this protocol. Similar hydrogenation methods can also be used in the hydrogenation of dutasteride which is also a 5α-reductase inhibitor commercialized under the trademark Avodart (**45**). Cilostamide, a selective and potent PDE3 inhibitor, was hydrogenated under the optimized conditions to give **46**, the structure of which was further confirmed by single-crystal X-ray diffraction.[39] The hydrogenation of **7** performed on a gram scale (Figure 3) was followed by a Suzuki coupling reaction to afford CYP11B2 inhibitor **47**. Overall, this reaction showed broad applicability to commonly used α,β-unsaturated compounds and was also compatible with early-stage and late-stage hydrogenation of bioactive molecules.

Deuterium-labeled compounds are of interest as diagnostic tools in drug discovery and probes in mechanistic studies. D_2O is the most available D source. We found that the addition of 10 (or 15) equivalents of D_2O under the optimized conditions resulted in dideuterated products. Several substrates were selected to examine the scope of this deuteration reaction. As shown in Figure 4, deuterated products **5-*d***, **7-*d***, **13-*d***, **15-*d***, **22-*d***, and **25-*d*** were successfully synthesized with excellent deuterium ratios using this protocol. Deuteration occurred selectively without affecting other bonds. The bioactive substrates were also tested and yielded the corresponding deuterium-labeled products **44-*d***, **45-*d***, and **46-*d***. Overall, this method provided ready access to dideuterium-labeled compounds starting from simple alkenes.

The reaction mechanism was first explored with irradiation on–off experiments (Figure S4). Conversion was suspended in the absence of irradiation, showing that the hydrogenation reaction is photochemical. Combined with control experiments, light on–off experiments and measured quantum yield $\Phi = 0.03$ (Figure S8 and S9), these results strongly suggested that alkene hydrogenation was a photoredox reaction.[40] An isotope labeling experiment was conducted to identify the hydrogen source for this hydrogenation reaction. As shown in Figure 5a, DCM-d_2 did not transfer deuterium into the product (entry 1), whereas toluene-d_8 gave a moderate deuterium ratio (entry 2). Detailed experiments using different deuterated toluene proved that both the methyl moiety and the phenyl moiety in toluene served as a hydrogen source in this reaction (entries 3 and 4). However, the deuteration ratio of the product **5** is still low even in the fully deuterated environment (entry 5). We speculated that the low deuteration ratio might be caused by the presence of a trace amount of H_2O in the system. In view of this hypothesis, D_2O was then added to the reaction system. As illustrated in Figure 4, the addition of 10 (or 15) equivalents of D_2O resulted in an extremely high deuterium ratio, which indicated that the hydrogen involved in this transformation is in the form of a proton. The reason for the formation of highly deuterated products might be that the H^+ (about 2 equiv) provided by *p*-xylene was much less than the D^+ (from 10 (or 15) equiv of D_2O) in the system. Such a large amount of D^+ enabled this photochemical hydrogenation to give highly deuterium labeled products. Furthermore, in the research process, we also found that when toluene was used as the solvent, some of the substrates would generate cyclization products, and the addition of a proton would have a fundamental impact on the selectivity of the cyclization process. For example, the observation of by-products **48** and **49** provided vital information for the reaction mechanism (Figure 5b).

To further probe the mechanism, the photochemical hydrogenation of **19S** with toluene was studied computationally using density functional theory (Figure 5c; for methods, see the Supporting Information). The mechanistic experiments led us to hypothesize that the photoexcitation of **9-HTXTF** allowed **50** (a TfOH-activated form of **19S**) and toluene to undergo two consecutive single-electron transfer steps with the photoexcited **9-HTXTF***, furnishing radical anion intermediate **51** and toluene radical cation **52**. The proton transfer between **51** and **52** then yielded a partially hydrogenated radical species **53**. Indeed, computations predicted an accessible ΔG_{tot} value of 21.4 kcal mol^{-1} for the simultaneous formation of transient intermediates **51** and

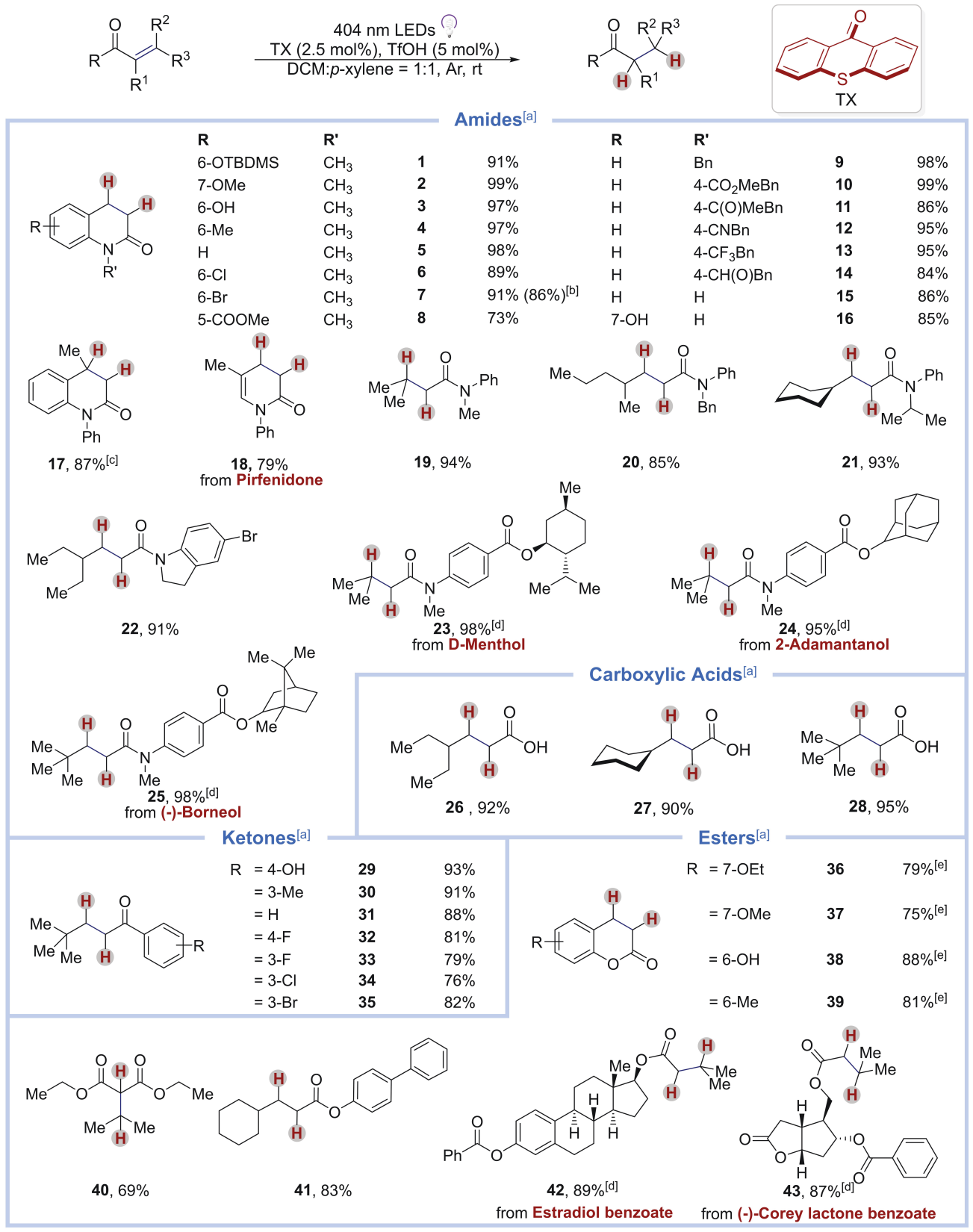

Figure 3. Substrate scope. [a] A mixture of S (0.2 mmol), TX (2.5 mol%), and TfOH (5 mol%) in a mixed solvent system of DCM and *p*-xylene (1 : 1, $c = 0.02$ M) was irradiated by 404 nm LEDs (60 W) at room temperature under an argon atmosphere (see the Supporting Information for full experimental details). Reported yields are for the isolated product. [b] Yield of the isolated product from a gram-scale reaction (1.500 g, 6.3 mmol). [c] TX (10 mol%) and TfOH (1.0 equiv) were used. [d] The reaction was carried out on a 0.1 mmol scale. [e] MeCN was used instead of DCM.

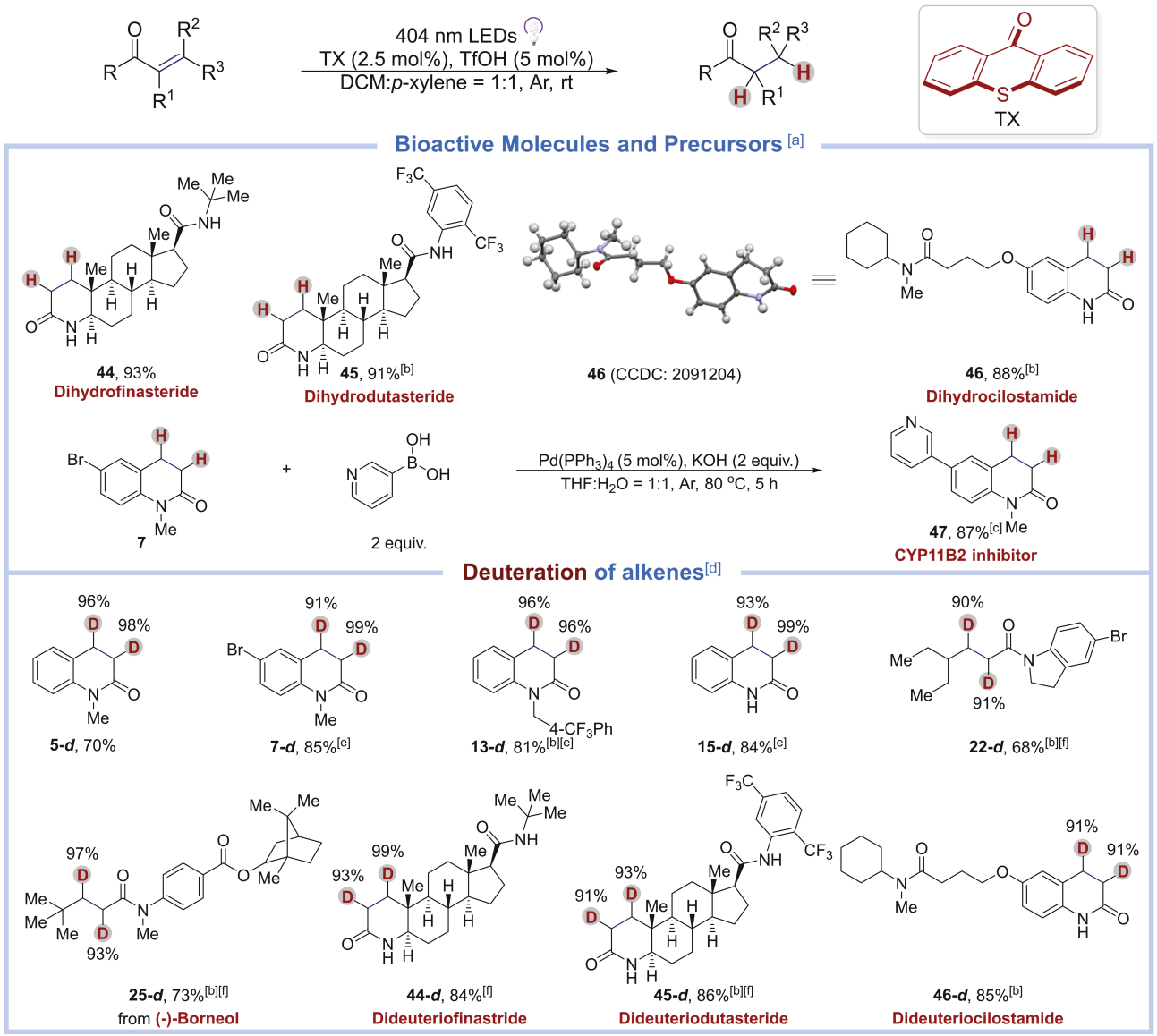

Figure 4. Hydrogenation of biomolecules and deuteration of alkenes. [a] A mixture of S (0.2 mmol), TX (2.5 mol%) and TfOH (5 mol%) in a mixed solvent of DCM and *p*-xylene (1 : 1, $c = 0.02$ M) was irradiated by 404 nm LEDs (60 W) at room temperature under an argon atmosphere (see the Supporting Information for full experimental details). Reported yields are for the isolated product. [b] The reaction was carried out on a 0.1 mmol scale. [c] A solution of **7** (0.2 mmol), pyridin-3-ylboronic acid (2 equiv), $Pd(PPh_3)_4$ (5 mol%), and KOH (2 equiv) in a mixed solvent system of THF and H_2O (1 : 1, $c = 0.1$ M) was stirred at 80 °C for 5 h. [d] A mixture of S (0.2 mmol), TX (2.5 mol%), TfOH (5 mol%) and D_2O (10 equiv) in a mixed solvent system of DCM and *p*-xylene (1 : 1, $c = 0.02$ M) was irradiated by 404 nm LEDs (60 W) at room temperature under an argon atmosphere. Reported yields are for the isolated product. [e] TX (10 mol%), TfOH (50 mol%) and D_2O (15 equiv) were used. [f] TX (10 mol%), TfOH (20 mol%) and D_2O (15 equiv) were used.

52, regardless of whether **9-HTXTF*** acted as photo-oxidant or photoreductant; this step was followed by favorable proton transfer from **52** to **51** with a large ΔG_{PT} value of $-42.2\ kcal\ mol^{-1}$ to afford **53**. Hence, the photoexcited **9-HTXTF*** fulfilled the energetic requirement for the proposed pathway. Furthermore, cyclic voltammetry measurement revealed that **9-HTXTF*** could oxidize xylene ($E_{1/2}(xylene\cdot^+/xylene) = +2.03$ V vs. SCE, $E_{1/2}(TX^*/TX^{\bullet-}) < E_{1/2}(xylene\cdot^+/xylene) < E_{1/2}$(**9-HTXTF***/**9-HTXTF**$^{\bullet-}$); for details, see the Supporting Information), and its oxidation capability was stronger than that of photoredox catalyst $(Acr^+–Mes)ClO_4$ ($E_{1/2}((Acr^+–Mes)ClO_4^*/(Acr^+–Mes)ClO_4^{\bullet-}) = +2.06$ V vs. SCE), which could oxidize toluene-type substrates by single-electron transfer.[41] Therefore, **9-HTXTF** preferentially serves as a photo-oxidant in the first step.

Subsequently, since the singly occupied frontier orbital of **53** could accept an electron, we envisaged that **53** should smoothly undergo photoreduction to afford an enolate species **54**, which could yield the product upon protonation. As described in the second step (see right-hand side of Figure 5c), our computations suggested that two pathways,

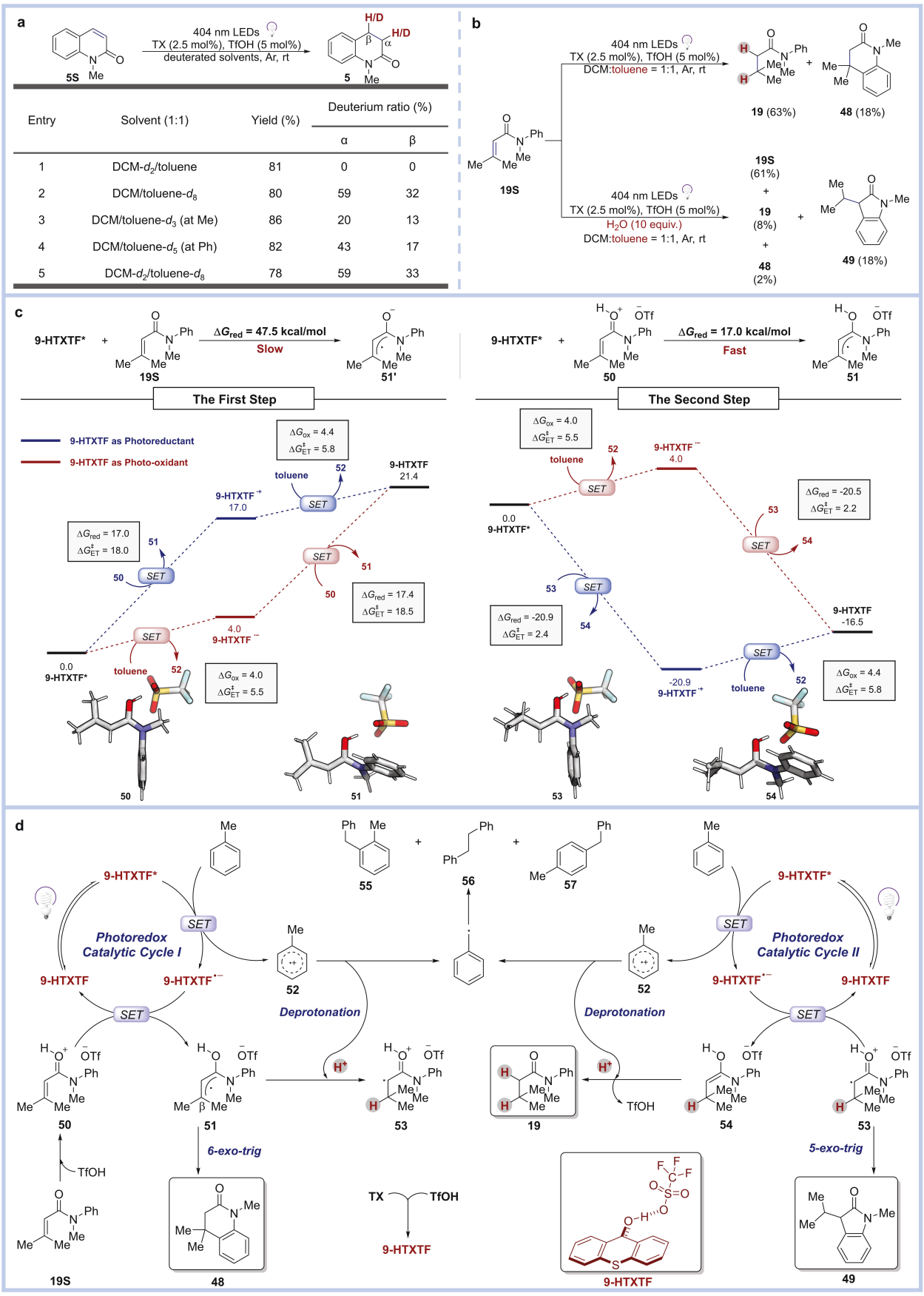

Figure 5. Mechanistic studies and proposed mechanism.

which begin with toluene oxidation and radical reduction (i.e., from **53** to **54**), respectively, are both energetically possible. Considering the short lifetime and low concentration of the radical intermediate **53** as well as the high concentration of toluene in the real reaction system, it seems possible that the second step also proceeds with toluene oxidation occurring prior to the reduction of **53**.

Overall, the results showed that the initial substrate reduction (generating **51**) and toluene oxidation (generating **52**) by the promoted electron and the associated electron hole in **9-HTXTF*** together constituted the energetically most demanding part of the reaction. These results are supported by calculations of electron transfer kinetics using Marcus–Hush theory, which predicts small kinetic barriers for all of the above-mentioned ET steps (see Figure 5c for $\Delta G^{\neq}_{ET}$ data). Further exploration of the roles of TfOH revealed that it protonated **19S** to allow the otherwise very unlikely substrate reduction ($\Delta G_{red} = 47.5\ kcal\,mol^{-1}$). Although dissociation of TfOH from **9-HTXTF**$^{\bullet-}$ would provide a strongly reducing radical anion **TX**$^{\bullet-}$, calculation of this process reveals a high energy of $35.9\ kcal\,mol^{-1}$ for the dissociation, which in turn strengthens the hypothesis that the photocatalyst operates as a complex. Combined with spectroscopic experiments, the results underscore the cooperative actions of **9-HTXTF** and TfOH as photococatalysts.

On the basis of the above mechanistic studies and literature precedent,[35,41,42] the mechanism is shown in Figure 5d. Irradiation of the **9-HTXTF** photocatalyst produces excited-state **9-HTXTF***. Single-electron oxidation of toluene by **9-HTXTF*** gives toluene radical cation **52** and the highly reductive **9-HTXTF**$^{\bullet-}$. The radical cation **52** is deprotonated to afford benzyl radical.[41] The following radical homocoupling or radical addition to toluene provides a series of dimerized toluene derivatives **55**–**57**,[43] which were detected by GC–MS analysis (Figure S5). Single-electron reduction of **50** by **9-HTXTF**$^{\bullet-}$ generates radical anion intermediate **51** and **9-HTXTF**. In the absence of a large amount of H^+, **51** can be converted into **48**[42] (for details, see Figure S7 in the Supporting Information). However, in the presence of excess proton source, selective protonation at the β site in **51** results in **53**, which can be converted into **49**[35] (for details, see Figure S7 in the Supporting Information). Similarly, single-electron reduction of **53** by **9-HTXTF**$^{\bullet-}$ yields the enolate species **54**, which can be protonated to form the final product **19**.

Conclusion

In conclusion, a typical photosensitizer, thioxanthone, was turned into a photoredox catalyst by the co-catalyst TfOH. The **9-HTXTF** catalyst showed very strong oxidative capability, a long singlet lifetime, and ready photoexcitation, all of which enabled the reduction of carbonylated alkenes. Xylene served as the hydrogen source in this reaction as proved by isotopic labeling experiments. Further studies on reduction reactions using **9-HTXTF** as the catalyst are currently in progress in our laboratory.

Acknowledgements

We acknowledge the Shanghai Science and Technology Committee (grant no. 21JM0010600 to H.G.) and the National Science Foundation of the USA (CHE-1764328 to K.N.H.) for financial support. We thank Haoliang Huang and Yaming Hao for providing electrochemical equipment. We thank Dahua Li and Zizhao Huang for providing fluorescence and phosphorescence spectrophotometers. We are grateful to Prof. Shoufei Zhu, Prof. Xiaosong Xue, Dr. Ying Dou, Dr. Binglin Wang, and Dr. Hua Tian for helpful discussions.

Conflict of Interest

The authors declare no conflict of interest.

Data Availability Statement

The data that support the findings of this study are available in the supplementary material of this article.

Keywords: Alkenes · Deuteration · Hydrogenation · Organocatalysis · Photoredox Catalysis

[1] H. B. Kagan, *Angew. Chem. Int. Ed.* **2012**, *51*, 7376–7382; *Angew. Chem.* **2012**, *124*, 7490–7497.
[2] P. G. Andersson, I. J. Munslow, *Modern Reduction Methods*, Wiley-VCH, Weinheim, **2008**.
[3] H. S. P. Rao, K. S. Reddy, *Tetrahedron Lett.* **1994**, *35*, 171–174.
[4] J. A. Osborn, F. H. Jardine, J. F. Young, G. Wilkinson, *J. Chem. Soc. A* **1966**, 1711–1732.
[5] R. Crabtree, *Acc. Chem. Res.* **1979**, *12*, 331–337.
[6] H. Lindlar, *Helv. Chim. Acta* **1952**, *35*, 446–450.
[7] M. Raney, *Ind. Eng. Chem.* **1940**, *32*, 1199–1203.
[8] Y. Gu, J. R. Norton, F. Salahi, V. G. Lisnyak, Z. Zhou, S. A. Snyder, *J. Am. Chem. Soc.* **2021**, *143*, 9657–9663.
[9] N. G. Léonard, P. J. Chirik, *ACS Catal.* **2018**, *8*, 342–348.
[10] R. Bigler, K. A. Mack, J. Shen, P. Tosatti, C. Han, S. Bachmann, H. Zhang, M. Scalone, A. Pfaltz, S. E. Denmark, S. Hildbrand, F. Gosselin, *Angew. Chem. Int. Ed.* **2020**, *59*, 2844–2849; *Angew. Chem.* **2020**, *132*, 2866–2871.
[11] Z. P. Vang, A. Reyes, R. E. Sonstrom, M. S. Holdren, S. E. Sloane, I. Y. Alansari, J. L. Neill, B. H. Pate, J. R. Clark, *J. Am. Chem. Soc.* **2021**, *143*, 7707–7718.
[12] P. Lu, X. Ren, H. Xu, D. Lu, Y. Sun, Z. Lu, *J. Am. Chem. Soc.* **2021**, *143*, 12433–12438.
[13] S. Weber, B. Stöger, L. F. Veiros, K. Kirchner, *ACS Catal.* **2019**, *9*, 9715–9720.
[14] J. Derosa, P. Garrido-Barros, J. C. Peters, *J. Am. Chem. Soc.* **2021**, *143*, 9303–9307.
[15] P. Stegner, C. Farber, U. Zenneck, C. Knupfer, J. Eyselein, M. Wiesinger, S. Harder, *Angew. Chem. Int. Ed.* **2021**, *60*, 4252–4258; *Angew. Chem.* **2021**, *133*, 4298–4304.
[16] D. M. Kaphan, M. S. Ferrandon, R. R. Langeslay, G. Celik, E. C. Wegener, C. Liu, J. Niklas, O. G. Poluektov, M. Delferro, *ACS Catal.* **2019**, *9*, 11055–11066.
[17] a) G. Brieger, T. J. Nestrick, *Chem. Rev.* **1974**, *74*, 567–580; b) R. A. W. Johnstone, A. H. Wilby, I. D. Entwistle, *Chem. Rev.* **1985**, *85*, 129–170.

[18] a) X. Cui, K. Burgess, *Chem. Rev.* **2005**, *105*, 3272–3296; b) F. Meemken, A. Baiker, *Chem. Rev.* **2017**, *117*, 11522–11569; c) L. Massaro, J. Zheng, C. Margarita, P. G. Andersson, *Chem. Soc. Rev.* **2020**, *49*, 2504–2522; d) H. Wang, J. Wen, X. Zhang, *Chem. Rev.* **2021**, *121*, 7530–7567.
[19] G. C. Welch, R. R. S. Juan, J. D. Masuda, D. W. Stephan, *Science* **2006**, *314*, 1124–1126.
[20] J. Lam, K. M. Szkop, E. Mosaferi, D. W. Stephan, *Chem. Soc. Rev.* **2019**, *48*, 3592–3612.
[21] J. Broggi, V. Jurcik, O. Songis, A. Poater, L. Cavallo, A. M. Slawin, C. S. Cazin, *J. Am. Chem. Soc.* **2013**, *135*, 4588–4591.
[22] B. K. Banik, K. J. Barakat, D. R. Wagle, M. S. Manhas, A. K. Bose, *J. Org. Chem.* **1999**, *64*, 5746–5753.
[23] Y. Wang, Z. Huang, X. Leng, H. Zhu, G. Liu, Z. Huang, *J. Am. Chem. Soc.* **2018**, *140*, 4417–4429.
[24] Y. Ito, H. Ohta, Y. M. Yamada, T. Enoki, Y. Uozumi, *Chem. Commun.* **2014**, *50*, 12123–12126.
[25] a) M. Flinker, H. Yin, R. W. Juhl, E. Z. Eikeland, J. Overgaard, D. U. Nielsen, T. Skrydstrup, *Angew. Chem. Int. Ed.* **2017**, *56*, 15910–15915; *Angew. Chem.* **2017**, *129*, 16126–16131; b) S. P. Cummings, T. N. Le, G. E. Fernandez, L. G. Quiambao, B. J. Stokes, *J. Am. Chem. Soc.* **2016**, *138*, 6107–6110.
[26] a) R. P. Rucker, A. M. Whittaker, H. Dang, G. Lalic, *J. Am. Chem. Soc.* **2012**, *134*, 6571–6574; b) R. F. Nystrom, W. G. Brown, *J. Am. Chem. Soc.* **1948**, *70*, 3738–3740; c) A. Giannis, K. Sandhoff, *Angew. Chem. Int. Ed. Engl.* **1989**, *28*, 218–220; *Angew. Chem.* **1989**, *101*, 220–222.
[27] a) H. Bauer, K. Thum, M. Alonso, C. Fischer, S. Harder, *Angew. Chem. Int. Ed.* **2019**, *58*, 4248–4253; *Angew. Chem.* **2019**, *131*, 4292–4297; b) Z. Wang, F. Ai, Z. Wang, W. Zhao, G. Zhu, Z. Lin, J. Sun, *J. Am. Chem. Soc.* **2015**, *137*, 383–389; c) N. Ishida, Y. Kamae, K. Ishizu, Y. Kamino, H. Naruse, M. Murakami, *J. Am. Chem. Soc.* **2021**, *143*, 2217–2220.
[28] E. E. van Tamelen, R. S. Dewey, R. J. Timmons, *J. Am. Chem. Soc.* **1961**, *83*, 3725–3726.
[29] a) J. Großkopf, T. Kratz, T. Rigotti, T. Bach, *Chem. Rev.* **2022**, *122*, 1626–1653; b) A. Y. Chan, I. B. Perry, N. B. Bissonnette, B. F. Buksh, G. A. Edwards, L. I. Frye, O. L. Garry, M. N. Lavagnino, B. X. Li, Y. Liang, E. Mao, A. Millet, J. V. Oakley, N. L. Reed, H. A. Sakai, C. P. Seath, D. W. C. MacMillan, *Chem. Rev.* **2022**, *122*, 1485–1542; c) M. J. Genzink, J. B. Kidd, W. B. Swords, T. P. Yoon, *Chem. Rev.* **2022**, *122*, 1654–1716; d) N. Holmberg-Douglas, D. A. Nicewicz, *Chem. Rev.* **2022**, *122*, 1925–2016; e) L. Capaldo, D. Ravelli, M. Fagnoni, *Chem. Rev.* **2022**, *122*, 1875–1924; f) K. Kwon, R. T. Simons, M. Nandakumar, J. L. Roizen, *Chem. Rev.* **2022**, *122*, 2353–2428; g) F. Strieth-Kalthoff, M. J. James, M. Teders, L. Pitzer, F. Glorius, *Chem. Soc. Rev.* **2018**, *47*, 7190–7202; h) C. Brenninger, J. D. Jolliffe, T. Bach, *Angew. Chem. Int. Ed.* **2018**, *57*, 14338–14349; *Angew. Chem.* **2018**, *130*, 14536–14547.
[30] a) L. N. Mendelsohn, C. S. MacNeil, L. Tian, Y. Park, G. D. Scholes, P. J. Chirik, *ACS Catal.* **2021**, *11*, 1351–1360; b) Y. Park, S. Kim, L. Tian, H. Zhong, G. D. Scholes, P. J. Chirik, *Nat. Chem.* **2021**, *13*, 969–976.
[31] a) M. L. Czyz, M. S. Taylor, T. H. Horngren, A. Polyzos, *ACS Catal.* **2021**, *11*, 5472–5480; b) A. Chatterjee, B. Konig, *Angew. Chem. Int. Ed.* **2019**, *58*, 14289–14294; *Angew. Chem.* **2019**, *131*, 14427–14432; c) C. Pac, M. Ihama, M. Yasuda, Y. Miyauchi, H. Sakurai, *J. Am. Chem. Soc.* **1981**, *103*, 6495–6497.
[32] B. A. Sandoval, P. D. Clayman, D. G. Oblinsky, S. Oh, Y. Nakano, M. Bird, G. D. Scholes, T. K. Hyster, *J. Am. Chem. Soc.* **2021**, *143*, 1735–1739.
[33] Deposition Number 2107208 (for **9-HTXTF**) contains the supplementary crystallographic data for this paper. These data are provided free of charge by the joint Cambridge Crystallographic Data Centre and Fachinformationszentrum Karlsruhe Access Structures service.
[34] I. A. MacKenzie, L. Wang, N. P. R. Onuska, O. F. Williams, K. Begam, A. M. Moran, B. D. Dunietz, D. A. Nicewicz, *Nature* **2020**, *580*, 76–80.
[35] Z. Liu, S. Zhong, X. Ji, G.-J. Deng, H. Huang, *ACS Catal.* **2021**, *11*, 4422–4429.
[36] Q. Xia, H. Tian, J. Dong, Y. Qu, L. Li, H. Song, Y. Liu, Q. Wang, *Chem. Eur. J.* **2018**, *24*, 9269–9273.
[37] K. Zhao, G. Seidler, R. R. Knowles, *Angew. Chem. Int. Ed.* **2021**, *60*, 20190–20195; *Angew. Chem.* **2021**, *133*, 20352–20357.
[38] a) H. Wang, H. Lian, J. Chen, Y. Pan, Y. Shi, *Synth. Commun.* **1999**, *29*, 129–134; b) H. M. Ali, A. A. Naiini, C. H. Brubaker, *Tetrahedron Lett.* **1991**, *32*, 5489–5492.
[39] Deposition Number 2091204 (for **46**) contains the supplementary crystallographic data for this paper. These data are provided free of charge by the joint Cambridge Crystallographic Data Centre and Fachinformationszentrum Karlsruhe Access Structures service.
[40] J. Davies, N. S. Sheikh, D. Leonori, *Angew. Chem. Int. Ed.* **2017**, *56*, 13361–13365; *Angew. Chem.* **2017**, *129*, 13546–13550.
[41] H. Liu, L. Ma, R. Zhou, X. Chen, W. Fang, J. Wu, *ACS Catal.* **2018**, *8*, 6224–6229.
[42] Z. H. Luan, J. P. Qu, Y. B. Kang, *J. Am. Chem. Soc.* **2020**, *142*, 20942–20947.
[43] See the Supporting Information for possible formation mechanisms of **55** and **57** to understand how aromatic hydrogens are incorporated into the product (Figure S6).

Manuscript received: August 5, 2022
Accepted manuscript online: September 15, 2022
Version of record online: October 26, 2022